View Article Online / Journal Homepage / Table of Contents for this issue

Electrostatic interactions for directed assembly of nanostructured materials: composites of titanium dioxide nanotubes with gold nanoparticles†

Jingxian Yu, Graham A. Rance and Andrei N. Khlobystov*

Received 27th July 2009, Accepted 18th September 2009
First published as an Advance Article on the web 19th October 2009
DOI: 10.1039/b915181h

Published on 19 October 2009. Downloaded by Michigan State University on 29/01/2016 16:37:24.

Interactions of titanium dioxide nanotubes (TiO_2NTs) with positively ($AuNP^+$s) and negatively charged ($AuNP^-$s) gold nanoparticles have been investigated using a combination of UV-Vis spectroscopy, ζ potential and transmission electron microscopy analyses. Possessing a negatively charged surface, TiO_2NTs show no attractive interactions with $AuNP^-$s, but readily form nanostructured composites with $AuNP^+$s. Using different ratios of TiO_2NT : $AuNP^+$, the overall charge of nanotube–nanoparticle composite can be tuned from positive through neutral to negative, which drastically affects the solubility of the resultant material in water. The charge of the nano-composite is related to the density of $AuNP^+$s adsorbed on the surface of the TiO_2NTs. At higher densities adsorbed nanoparticles interact with each other and exhibit a red-shift of their surface plasmon resonance, the magnitude of which increases with the density of $AuNP^+$s. This methodology enables precise control over the composition, charge and structure of nanotube–nanoparticle materials.

Introduction

With the development of nanoscience and nanotechnology, a wide range of different materials (metals, metal oxides and semiconductors) have been fabricated in a number of diverse morphologies, including nanoparticles,[1] nanotubes, nanorods, nanofibers, nanosheets,[2] nanoribbons[3,4] and nanorings.[5,6] These fascinating nanoscale structures are of significant interest because their physicochemical properties differ from those of the bulk materials, and thus can be exploited for microelectronics, optoelectronics, catalysis, information storage and other applications. Controlled manipulation of nanoscale building blocks for the purpose of nanodevice fabrication, however, is still a big challenge. Bottom-up assembly of mesoscopic structures from nanoscopic building blocks is one of the strategies developed to address this problem and numerous examples exist within the scientific literature. Carbon nanotubes, for instance, have been employed as a scaffolding material for the construction of complex one-, two- and three-dimensional nanocomposites with nanoparticles.[7] A variety of non-covalent approaches, where the interactions between nanotubes and nanoparticles are mediated by forces, such as van der Waals interactions,[8] electrostatic interactions,[9] π–π stacking interactions[10] or hydrophobic interactions,[11] have been investigated with the aim of enhancement of the functional properties of the nanoscale building blocks within the composite structures. Of these non-covalent strategies, electrostatic interactions are particularly suitable for this purpose, as they are long-range, reversible and tuneable by external stimuli, such as pH and ionic strength.[12–15]

The use of electrostatic interactions between carbon nanotubes and nanoparticles has led to the formation of a variety of fascinating architectures, but critically depends upon the possession of inherent charge. For nanoparticles, the presence of charge is essential for their stability as discrete colloidal species and can be controlled by conditions of the synthetic procedure. For carbon nanotubes, however, charge is introduced post-synthesis and this is often done either through attachment of surfactants and polymers or by chemical functionalisation. For example, Jiang *et al.*[16] achieved a uniform distribution of gold nanoparticles on nitrogen-doped carbon nanotubes which were modified with a cationic polyelectrolyte. The negatively charged gold nanoparticles were attracted by electrostatic forces to pre-adsorbed positively charged polymer chains and distributed uniformly along the sidewalls and tips of the carbon nanotubes. In an analogous study, Correa-Duarte and Liz-Marzan[17] used two successive polyelectrolyte layers on multi-walled carbon nanotubes to promote the deposition of $Au@SiO_2$ core–shell nanoparticles. The chemical functionalisation of nanotubes, yielding either positively or negatively charged cylindrical nanostructures depending on the specific treatment employed, has also lead to the construction of nano-composites with a variety of nanoparticles, including, but not limited to, those composed of cadmium sulfide,[18] chitosan[19] and Prussian blue.[20] Moreover, widely applied nanofabrication methods, such as the layer-by-layer deposition technique,[21–23] also depend on the existence of electrostatic interactions between functionalised nanotubes and nanoparticles.

In our study, we have extended the basic principles of electrostatic interactions between nanotubes and nanoparticles to assess the construction of composites of titanium dioxide nanotubes (TiO_2NTs) and gold nanoparticles (AuNPs). TiO_2NTs, materials which have shown promise for a broad range of potential applications in hydrogen sensors, adsorbents, photocatalysis, electrocatalysis, mesoporous catalyst supports,[24,25]

School of Chemistry, University of Nottingham, University Park, Nottingham, UK NG7 2RD. E-mail: Andrei.Khlobystov@nottingham.ac.uk
† Electronic supplementary information (ESI) available: Fig. S1–S5. See DOI: 10.1039/b915181h

 This journal is © The Royal Society of Chemistry 2009

View Article Online

Published on 19 October 2009. Downloaded by Michigan State University on 29/01/2016 16:37:24.

solar cell photosensitisers and a new generation of electrode materials for energy storage,[26–32] offer many advantages over carbon nanotubes, including ease of preparation by simple alkaline hydrothermal treatment,[31,32] high suspension stability in aqueous media due to surface hydrophilicity and useful electronic properties, possessing a wide band gap (around 3.2 eV[26]). The use of AuNPs as model 0D nanostructures offers many advantages for controlling electrostatic interactions, including control of both particle size and surface charge. Furthermore, the assembly of TiO_2NT–AuNP hybrid materials is relatively unexplored, with only a small number of reports focussing on enhancing the properties of TiO_2NTs, typically by chemical functionalisation of the nanotube surface.[33] It has been shown that the photocatalytic activity of these structures can be significantly improved using such an approach, with the resulting nanostructures exhibiting functional optical properties, shifting the absorbance of the TiO_2NTs into the visible range.[34–37] For example, Schmuki and co-workers[37] prepared Ag ($\sim 10 \pm 2$ nm) or Au ($\sim 28 \pm 3$ nm) nanoparticles decorated with TiO_2NTs using a metal sputtering system. They found that the AuNP–TiO_2NT and AgNP–TiO_2NT composites are highly efficient for the UV-light induced photocatalytic decomposition of a model organic pollutant. However, the effect of electrostatic interactions between preformed TiO_2NTs and AuNPs has not been systematically studied and that was the motivation for this study.

Experimental

All common reagents and solvents were purchased from Sigma-Aldrich UK, unless stated otherwise, and used without further purification. Water was purified (>18 MΩ cm) using a Barnstead NANOPure II system. All experimental procedures were performed using conventional glass apparatus, unless otherwise stated. The preparation and use of gold nanoparticles required glassware to be cleaned with a mixture of concentrated hydrochloric and nitric acids (3 : 1, 'aqua regia') and rinsed with deionised water prior to use. UV-Vis spectra were recorded in 10 mm quartz cuvettes using a Perkin-Elmer Lambda 25 UV-Vis spectrophotometer at a scan rate of 120 nm min^{-1} over the wavelength range 400–800 nm. The hydrodynamic nanoparticle size and surface ζ potential were determined using a ZetaSizer Nano ZS (Malvern Instruments Inc. UK) utilising dynamic light scattering (DLS) and laser Doppler velocitometry (LDV) respectively. A minimum of five measurements for each sample were taken to ensure statistical relevance. Unless stated otherwise, comparative values of ζ potential were recorded using solutions of identical pH and ionic strength. Transmission electron microscopy (TEM) images were taken using a JEOL JEM-2100F field emission gun microscope at room temperature. Samples were prepared by depositing several drops of aqueous suspension onto a holey carbon film mounted on a copper TEM grid (Agar Scientific UK) and dried under a stream of nitrogen.

Citrate-stabilised gold nanoparticles (AuNP@Citrate) were prepared using a modified aqueous citrate reduction method whereby tannic acid was used as an additional reducing agent.[38] Typically, an aqueous solution of hydrogen tetrachloroaurate (1 mL, 1 wt% stock solution) was diluted with deionised water (79 mL) and heated to 60 °C. A separate aqueous solution containing tannic acid (1 mL, 1 wt% stock soltuion) and trisodium citrate dihydrate (4 mL, 1 wt% stock solution) diluted with deionised water (3 mL) was additionally heated to 60 °C. The two solutions were next combined and heated at 60 °C until the reaction had gone to completion, as indicated by a permanent ruby red colour of the solution.

4-(Dimethylamino)pyridine (DMAP) stabilised gold nanoparticles (AuNP@DMAP) were prepared using the method reported by Lennox and co-workers.[39–36] To hydrogen tetrachloroaurate (125 mg) was added deionised water (10 mL) and the mixture stirred for 10 min yielding a bright yellow solution. A separate solution containing tetraoctylammonium bromide (765 mg) in toluene (25 mL) was also stirred for 10 min and then added with vigorous stirring to the aqueous gold solution, resulting in a coloured biphasic mixture. A further solution of sodium borohydride (131 mg) in deionised water (8 mL) was stirred for 10 min and then added to the biphasic mixture, resulting in an instant colour change in the organic layer from orange to ruby red/purple. This was then vigorously stirred for 48 h at room temperature. The biphasic mixture was then separated, retaining the organic layer which was washed with water (3×20 mL) and dried over anhydrous sodium sulfate. The organic layer was next diluted with toluene (35 mL) and added to an aqueous solution of DMAP (730 mg) in deionised water (60 mL) and left for 1 h at room temperature with no agitation. The resultant biphasic mixture was separated, retaining the aqueous phase to yield a ruby red solution which was then diluted 10-fold with deionised water and stored at 4 °C for further use.

The preparation of TiO_2 nanotubes (TiO_2NTs) was based on the alkaline hydrothermal transformation developed by Kasuga and co-workers.[31,32] Titanium dioxide particles (300 mg, anatase, 99.8%) were added an to aqueous solution of sodium hydroxide (80 mL, 10 M) and the mixture was vigorously stirred for 30 min at room temperature. The resulting white slurry was next split into two identical (40 mL) portions, transferred into hydrothermal reactors (Parr Instrument Co. USA) and heated at 140 °C for 24 h. This was filtered through a PTFE membrane (0.45 μm, Aldrich), washed with copious water until pH ~7, then washed with sulfuric acid (50 mL, 0.05 M) for 30 min, followed by vacuum-drying at 80 °C. The structure of TiO_2NTs was determined by high resolution transmission electron microscopy (Fig. 1). All nanotubes appear as concentric cylindrical tubules with open-ends. Quantitative analysis of the morphological parameters was undertaken: mean inner and outer diameters of

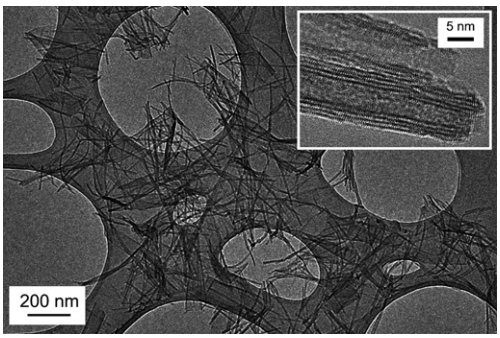

Fig. 1 TEM images of TiO_2 nanotubes. Inset is a high-magnification TEM image.

View Article Online

Published on 19 October 2009. Downloaded by Michigan State University on 29/01/2016 16:37:24.

4.6 ± 0.4 and 10.9 ± 0.4 nm respectively and a mean length of 538.8 ± 23.8 nm was determined. Similar structural parameters of TiO_2NT have been reported by other research groups.[30,31,40]

Different quantities of TiO_2NTs (0–15 mg) were added into a series of vials containing deionised water (2 mL) and treated briefly in an ultrasonic bath to prepare suspensions. AuNP@-Citrate and AuNP@DMAP (2 mL respectively) were then separately added into each suspension of TiO_2NTs. The resultant mixtures were allowed to equilibrate and then characterised by complementary UV-Vis spectroscopic and light scattering. Sediments were taken for transmission electron microscopic analysis after the supernatants were carefully removed by pipette.

Results and discussion

In order to evaluate the effects of electric charge on the interactions of TiO_2NTs with nanoparticles, we have prepared two types of AuNP with similar mean size and dispersity (Fig. 2), but with different surface functionalities and thus different surface charges. Gold nanoparticles coated with 4-(dimethylamino)pyridine (mean diameter = 8.45 ± 1.23 nm) are expected to be positively charged, whereas those coated with citrate (mean diameter = 8.72 ± 1.26 nm) should be negatively charged. The relative sign and magnitude of effective surface charge was verified by ζ potential measurements. It is important that the size distributions of the two samples of AuNPs are similar, therefore ensuring that any differences in the interactions of TiO_2NTs and these nanoparticles can be solely attributed to the particle charge.

The surface ζ potentials at neutral pH have been measured −40.7 ± 3.6 and +25.2 ± 1.8 mV for AuNP@Citrate and AuNP@DMAP respectively (Fig. 3). In the AuNP@Citrate system, negatively charged citrate ions are adsorbed at the monovalent gold surface[41,42] thereby stabilising individual nanaoparticles by electrostatic repulsion.[43,44] In the AuNP@D-MAP system, 4-(dimethylamino)pyridine forms a labile donor–acceptor complex with the gold surface atoms through the endocyclic nitrogen atom with the positive surface charge arising from a combination of partial protonation of the exocyclic nitrogen atom that extends away from the nanoparticle surface

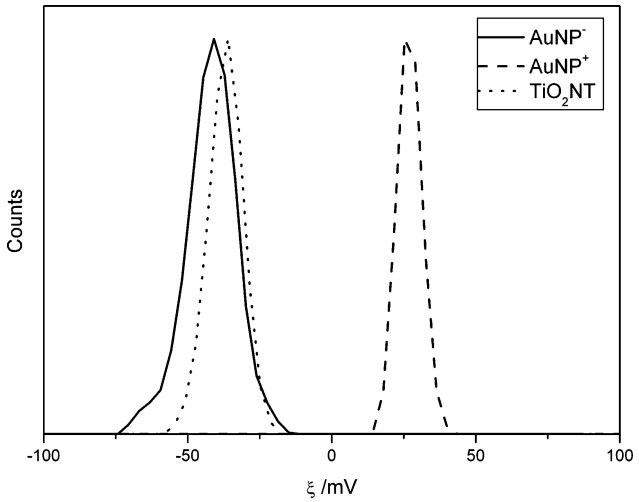

Fig. 3 Nanoparticle surface ζ potential measurements for citrate stabilised gold nanoparticles ($AuNP^-$s), 4-(dimethylamino)pyridine stabilised gold nanoparticles ($AuNP^+$s), and titanium dioxide nanotubes in deionised water (pH = 7).

and resonance stabilisation.[39,45] Owing to the opposite surface charges carried by AuNP@Citrate and AuNP@DMAP, they are simply denoted as $AuNP^-$ and $AuNP^+$ respectively in the remaining text. For TiO_2NT, the mean surface ζ potential was found to be −35.8 ± 2.6 mV at pH = 7. Bavykin and co-workers[46] reported an average surface ζ potential of −42 mV for titanium dioxide nanotubes in water, which is in a good agreement with our measurements. Thus both TiO_2NT and $AuNP^-$ are negatively charged, while $AuNP^+$ are positively charged and as such expected to form long-range attractive interactions with TiO_2NT.

In order to investigate the interactions between negatively charged titanium dioxide nanotubes and two oppositely charged gold nanoparticle systems, different quantities of titanium dioxide nanotubes were added into a series of vials each containing the same volume (2 mL) of gold nanoparticle solution. The mixtures of titanium dioxide nanotubes and gold nanoparticles were next allowed to equilibrate overnight (Fig. 4). For

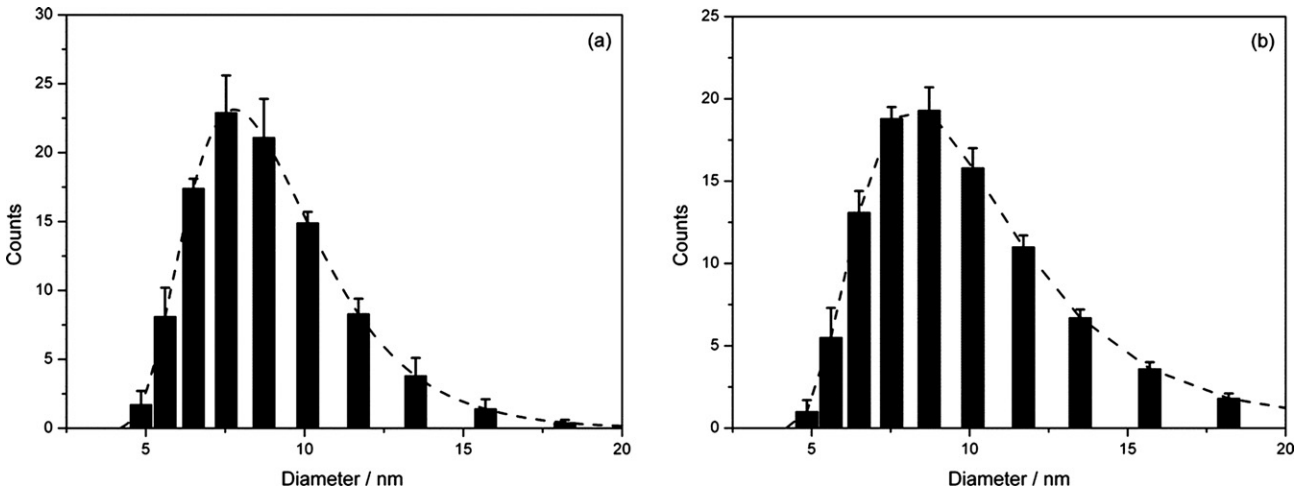

Fig. 2 Particle size distributions measured by dynamic light scattering for (a) citrate stabilised and (b) 4-(dimethylamino)pyridine stabilised gold nanoparticles. Error bar for each data point indicates the standard deviation over 5 measurements.

 This journal is © The Royal Society of Chemistry 2009

View Article Online

Published on 19 October 2009. Downloaded by Michigan State University on 29/01/2016 16:37:24.

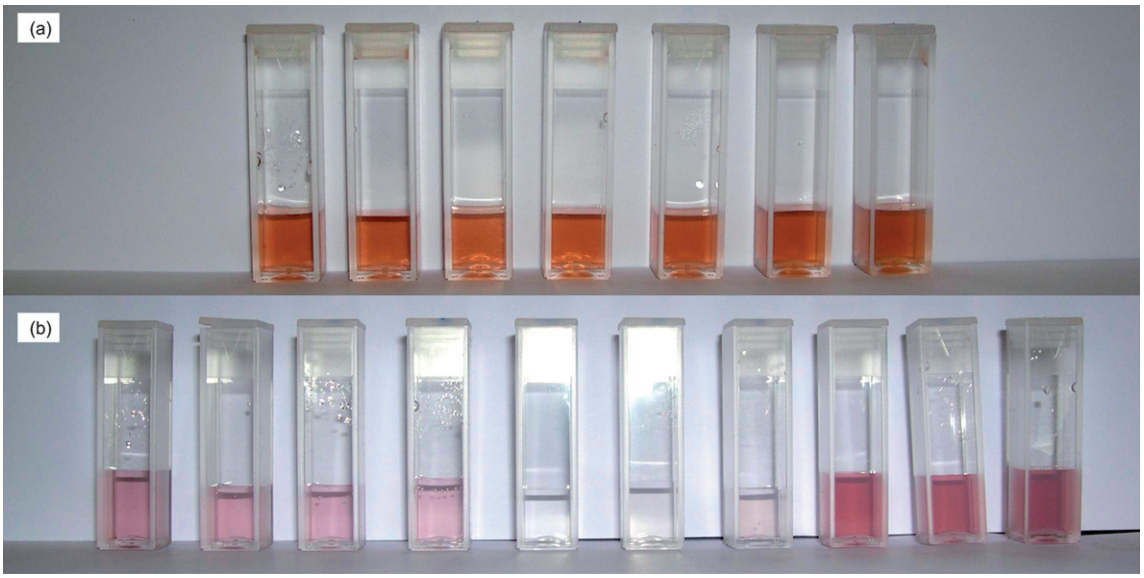

Fig. 4 Photographs of supernatant solutions taken (a) for $AuNP^{-}$–TiO_2NT system with TiO_2NT : $AuNP^{-}$ mass ratios (from left to right) 0, 0.8, 1.6, 4.1, 9.9, 42.0 and 72.5, and (b) for $AuNP^{+}$–TiO_2NT system with TiO_2NT : $AuNP^{+}$ mass ratios (from left to right) 0, 0.3, 0.8, 1.5, 2.5, 5.1, 10.8, 22.4, 39.8 and 72.5.

the titanium dioxide nanotube and negatively charged gold nanoparticle ($AuNP^{-}$–TiO_2NT) system, the colour of supernatants stays nearly the same regardless of the amount of TiO_2NT added. However, in the titanium dioxide nanotube and positively charged gold nanoparticle ($AuNP^{+}$–TiO_2NT) system, drastic colour transformations were observed. As the amount of TiO_2NT gradually increases, the colour of the $AuNP^{+}$–TiO_2NT system changes from pink (no TiO_2NT), to light pink, to colourless (TiO_2NT : $AuNP^{+}$ mass ratio = 2.5), to light pink, and finally to wine-red (TiO_2NT : $AuNP^{+}$ mass ratio = 72.5). It is also important to note that for the $AuNP^{+}$–TiO_2NT system some precipitate is formed, the colour and amount of which is dependent on the amount of TiO_2NP added to the nanoparticles.

In an attempt to quantify the colour changes observed upon addition of TiO_2NT, UV-Vis spectra of the supernatants of each sample have been recorded (Fig. 5). In the $AuNP^{-}$–TiO_2NT system (Fig. 5a), the addition of TiO_2NT causes a gradual increase in the absorbance across the UV region of the spectrum (Fig. S1†) and this increase is directly proportional to the amount of TiO_2NT added into the system (Fig. 5c and S2a†). At the same time an absorption peak at 520 nm associated with $AuNP^{-}$ plasmon resonance remains virtually unchanged at any concentration of TiO_2NT. The ζ potential of the $AuNP^{-}$–TiO_2NT system stays approximately at the same negative value for all the samples (Fig. 6a), which confirms that there are no attractive interactions between negatively charged $AuNP^{-}$ and TiO_2NT, and so each absorption spectrum of $AuNP^{-}$–TiO_2NT represents a simple superposition of $AuNP^{-}$ and TiO_2NT component spectra.

In the $AuNP^{+}$–TiO_2NT system (Fig. 5b), the increase in concentration of TiO_2NT causes significant changes in the $AuNP^{+}$ plasmon peak centred at 520 nm. As the TiO_2NT : $AuNP^{+}$ mass ratio increases from 0 to 2.5, the plasmon peak decreases in intensity reaching zero for TiO_2NT : $AuNP^{+}$ mass ratio = 2.5. Further addition of TiO_2NT leads to a gradual recovery of the plasmon peak at 520 nm as well as the increase of absorbance in the UV-range associated with TiO_2NT. The complicated shape of the dependence of absorbance of supernatant upon the amount of TiO_2NT (Fig. 5d and S2b†) indicates strong attractive interactions between positively charged $AuNP^{+}$ and TiO_2NT. This hypothesis is confirmed by studying the ζ potential of the $AuNP^{+}$–TiO_2NT system (Fig. 6b). For small amounts of TiO_2NT (TiO_2NT : $AuNP^{+}$ mass ratio < 1.9) the charge of species present in the supernatant is positive and decreases as more TiO_2NT is added to the mixture. As expected, positively charged nanoparticles are attracted to negatively charged nanotubes forming a nanoparticle–nanotube composite whose overall charge is lower than the charges of the individual components. The quenching of the positive charge of $AuNP^{+}$ with the negative change of TiO_2NT causes precipitation of the nanoparticle–nanotube composite structures, which is manifested in the decrease of absorption intensity of the supernatant (Fig. 5b). The isoelectric point estimated from ζ-potential measurements is reached at TiO_2NT : $AuNP^{+}$ mass ratio = 1.9, where the effective ζ potential of the system becomes zero. The mass ratio at the isolelectric point is close to that at the point of minimum optical absorbance of solution (Fig. 5b), which confirms that the solubility of TiO_2–AuNP composite correlates strongly with its overall charge. Further addition of TiO_2NT beyond the isoelectric point reverses the charge of the system as it becomes dominated by the negative charge of TiO_2NT. As the ζ potential value becomes more negative, the intensity of the absorption increases proportionally to the concentration of nanotubes.

Transmission electron microscopy allows a more detailed analysis of the nano-composite structures formed from TiO_2NT and AuNP. In the $AuNP^{-}$–TiO_2NT system (Fig. 7a), very few $AuNP^{-}$ particles can be found attached to nanotubes. This supports the spectroscopic observations that there are no significant attractive interactions between the negatively charged

View Article Online

Published on 19 October 2009. Downloaded by Michigan State University on 29/01/2016 16:37:24.

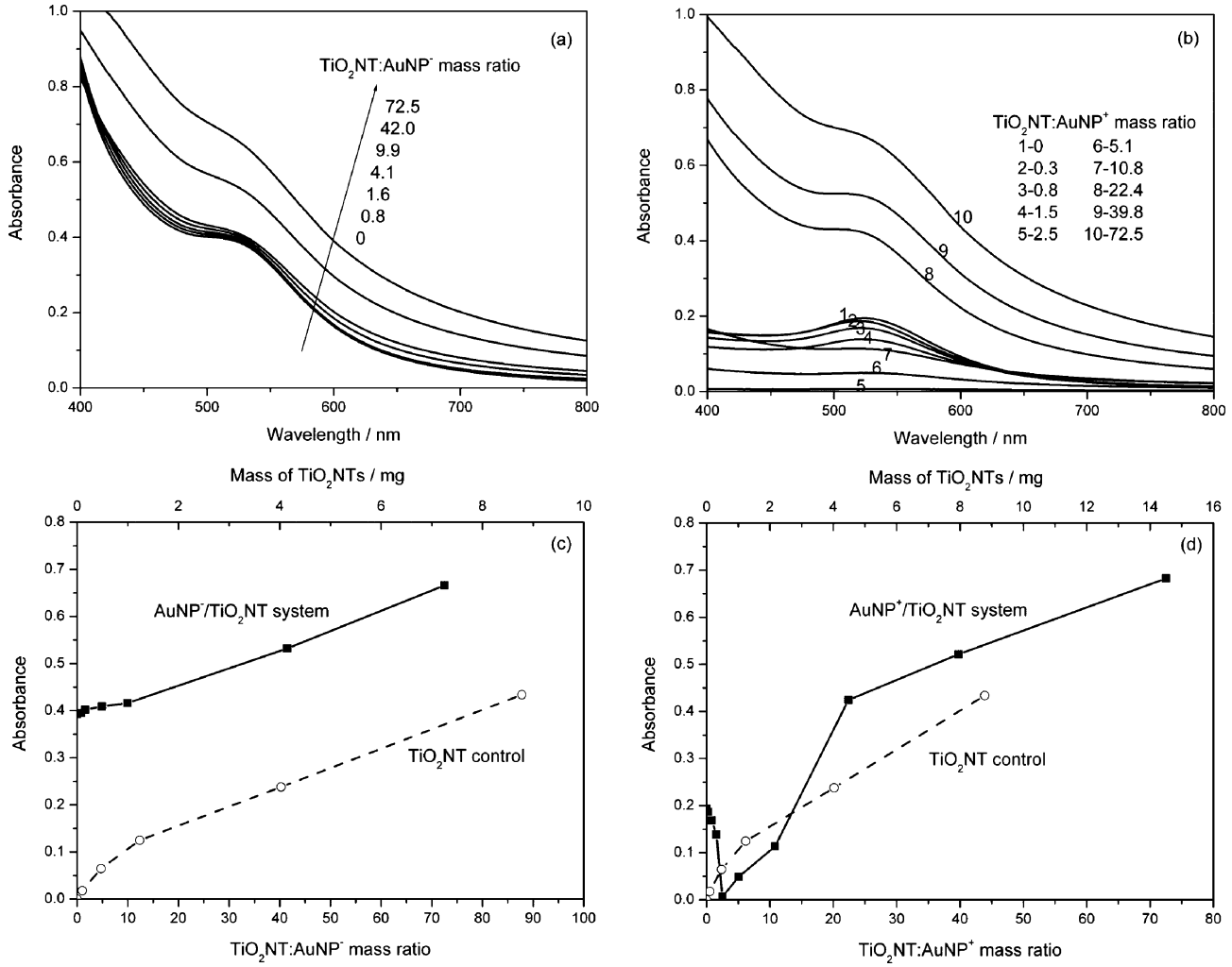

Fig. 5 UV-Vis spectra of supernatant solutions taken from (a) $AuNP^{-}$–TiO_2NT system and (b) $AuNP^{+}$–TiO_2NT system. Dependence of UV-Vis absorbance at 520 nm on TiO_2NT : AuNP mass ratio for (c) $AuNP^{-}$–TiO_2NT and (d) $AuNP^{+}$–TiO_2NT systems.

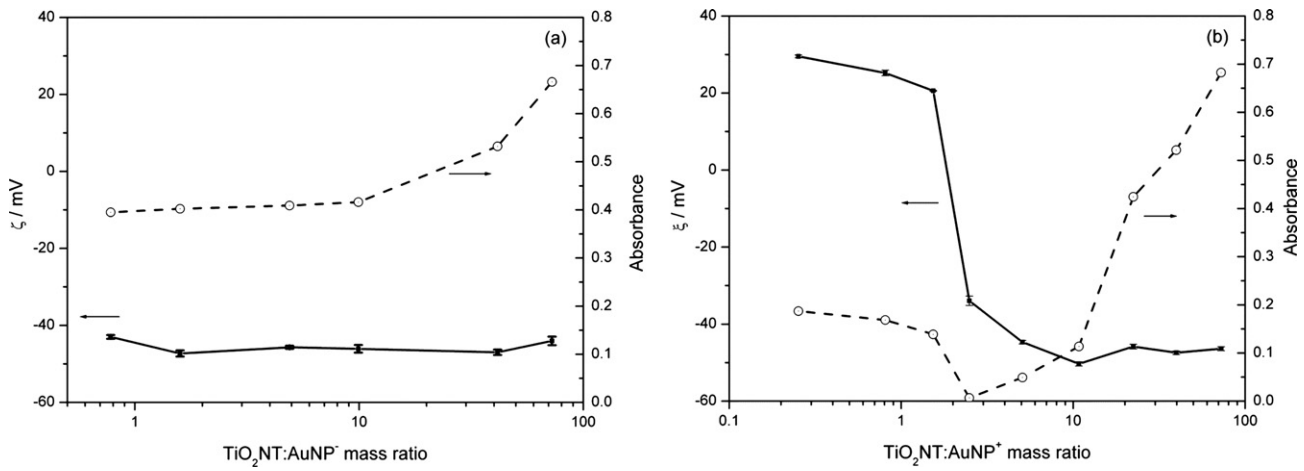

Fig. 6 ζ potential and optical absorbance measurements of supernatants for the (a) $AuNP^{-}$–TiO_2NT and (b) $AuNP^{+}$–TiO_2NT systems. Error bar for each data point indicates the standard deviation over 5 measurements.

$AuNP^{-}$ and TiO_2NT. The electrostatic repulsive force prevents citrate-stabilised gold nanoparticles from adsorbing on the surface of TiO_2NT. Under the same conditions, $AuNP^{+}$ adsorb readily on TiO_2NT (Fig. 7b), so that nanotubes are completely and evenly covered by nanoparticles forming hard contact with the TiO_2NT surface. This is consistent with the fact that $AuNP^{+}$ are strongly attracted to TiO_2NT by electrostatic forces. From the high magnification TEM (Fig. 7b, inset) it can be seen that

 This journal is © The Royal Society of Chemistry 2009

View Article Online

Published on 19 October 2009. Downloaded by Michigan State University on 29/01/2016 16:37:24.

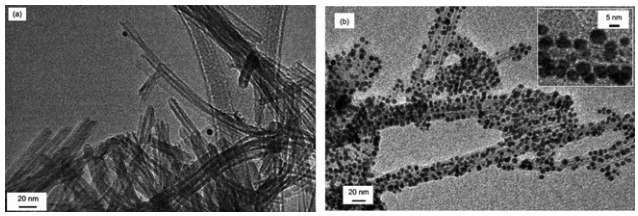

Fig. 7 TEM images for the precipitates taken from (a) $AuNP^{-}$–TiO_2NT and (b) $AuNP^{+}$–TiO_2NT systems. The inset is a high magnification TEM image for $AuNP^{+}$–TiO_2NT sample.

the average gold nanoparticle density for $AuNP^{+}$ on TiO_2NT surface is 43 ± 5 nanoparticles per 100 nm of the nanotube length, so that before reaching the isoelectric point all the nanotube surfaces are virtually saturated with $AuNP^{+}$. After the isoelectric point the density of nanoparticles adsorbed on nanotubes decreases with the concentration of TiO_2NT in the system. For example, for the TiO_2NT : $AuNP^{+}$ mass ratio = 10.8 the nanoparticle density on nanotubes is 10 ± 6 nanoparticle per 100 nm (Fig. S3a†), and for TiO_2NT : $AuNP^{+}$ = 39.8 it is as low as 1–2 nanoparticles per 100 nm of nanotube length (Fig. S3b†). It also should be noted that at higher nanotube concentrations, the nanoparticle distribution on nanotubes observed by TEM becomes less homogeneous than at the isoelectric point. This observation is related to the fact that beyond the isoelectric point the solution will always contain TiO_2NT that are only sparsely decorated with AuNP, and which can become incorporated within TEM samples during the separation of precipitate from supernatant.

Based on the above observations, a schematic mechanism of the interactions between $AuNP^{+}$ and TiO_2NT has been proposed (Fig. 8). If a small amount of TiO_2NT is added (Fig. 8b), all TiO_2NT precipitate out as charge neutral nanoparticle–nanotube composite structures. Before the isoelectric point, the supernatant contains only $AuNP^{+}$ which are gradually sequestered by TiO_2NT added to the mixture. At the isoelectric point (Fig. 8c), all gold nanoparticles and all TiO_2NT precipitate out, so that supernatant is colourless. If the concentration of TiO_2NT in the system increases further beyond the isoelectric point, some of the nanoparticles will be redistributed between precipitated nanotubes and newly added nanotubes, which are now present in excess, so that the overall charge of the system is negative (Fig. 8d). Nanotubes with a low coverage of nanoparticles carry some uncompensated negative charge making them sufficiently buoyant and thus the supernatant will now contain $AuNP^{+}$ sparsely adsorbed on TiO_2NT (Fig. 8d–f and S4†). Consequently, after the isoelectric point, the absorption intensity of the supernatant will increase with each new portion of TiO_2NT added.

Our TEM studies have shown that the density of AuNP on TiO_2NT can be tuned by simply adjusting the amount of TiO_2NT. It is interesting to correlate the nanoparticle plasmon energy with the density of AuNP and the average inter-particle separation in the nanotube–nanoparticle composites. Composites with different ratios of TiO_2NT : $AuNP^{+}$ were collected and

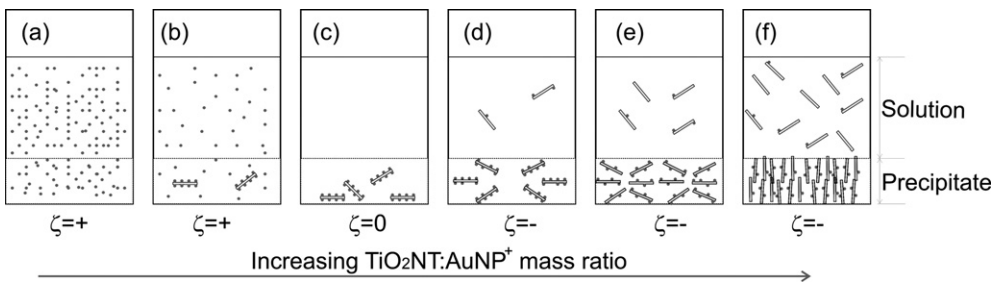

Fig. 8 A schematic representation of the mechanism of interactions between $AuNP^{+}$ and TiO_2NT. (—) TiO_2NT and (●) $AuNP^{+}$.

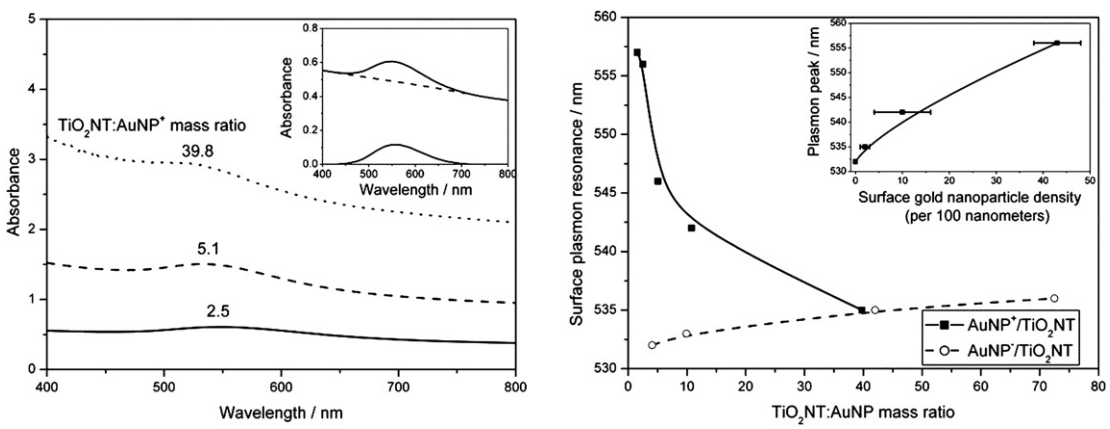

Fig. 9 (a) UV-Vis absorption of nanotube–nanoparticle composites taken from $AuNP^{+}$–TiO_2NT system with different TiO_2NT : AuNP ratios. The inset shows the plasmon peak before and after subtraction of the background absorption. (b) Dependence of plasmon peak position on the TiO_2NT : AuNP mass ratio. The inset shows the relationship between the plasmon peak position and AuNP density on TiO_2NT.

View Article Online

Published on 19 October 2009. Downloaded by Michigan State University on 29/01/2016 16:37:24.

re-dispersed in pure water again for optical absorption measurements. The absorption due to TiO_2NT was subtracted from the UV-Vis spectra of the composites (Fig. 9a and S5†), the intensities of $AuNP^+$ plasmon peaks were normalised and the plasmon peak positions for different samples were correlated with the TiO_2NT : AuNP mass ratio (Fig. 9b) and the particle density on nanotubes (Fig. 9b, inset). For the $AuNP^-$–TiO_2NT system, with no attractive interactions between nanotubes and nanoparticles, the $AuNP^-$ plasmon resonance peak position remains essentially the same. However, in the $AuNP^+$–TiO_2NT system, the $AuNP^+$ plasmon peak exhibits a clear red-shift as the density of nanoparticles on nanotubes increases (Fig. 9b, inset). Previously it has been shown that if the separation between metallic nanoparticles is smaller than their radii, plasmonic coupling can occur, an effect which will manifest itself as significant changes in their absorption spectra.[47] For example, Mirkin and co-workers [48,49] have demonstrated that the nanoparticle plasmon frequency is inversely dependent on the length of the oligonucleotide bridging two nanoparticles.[50] Similar observations have been reported by Decher's group for other types of gold nanoparticles[51] and by Heath's group for silver nanoparticles.[52] The previous studies carried out for different nanoparticle composite materials are in a good agreement with our measurements. Therefore, the position of the AuNP plasmon resonance can be used to measure the average inter-particle separation and thus to estimate the density of nanoparticles adsorbed on TiO_2NT.

Conclusions

Electrostatic forces are amongst most effective interactions that can be employed for non-covalent assembly of nanostructured composite materials. In this study we have demonstrated that the charge–charge interactions enable precise control over the composition and structure of assemblies of gold nanoparticles and titanium dioxide nanotubes. Being chemically and thermally stable wide band gap semiconductors TiO_2 nanotubes are currently viewed as useful materials for supporting catalytically, optically or magnetically active nanoparticles. Using Au nanoparticles as a model, we have devised a methodology for controlled deposition of nanoparticles on TiO_2 nanotube surfaces.

Acknowledgements

This work was supported by the EPSRC, European Science Foundation, Nottingham Nanotechnology and Nanoscience Centre, and the Royal Society.

References

1 M. C. Daniel and D. Astruc, *Chem. Rev.*, 2004, **104**, 293–346.
2 H. G. Yang, G. Liu, S. Z. Qiao, C. H. Sun, Y. G. Jin, S. C. Smith, J. Zou, H. M. Cheng and G. Q. Lu, *J. Am. Chem. Soc.*, 2009, **131**, 4078–4083.
3 J. M. Kinder, J. J. Dorando, H. T. Wang and G. K. L. Chan, *Nano Lett.*, 2009, **9**, 1980–1983.
4 H. T. Chen, S. J. Xiong, X. L. Wu, J. Zhu, J. C. Shen and P. K. Chu, *Nano Lett.*, 2009, **9**, 1926–1931.
5 M. Z. Yin, Y. J. Cheng, M. Y. Liu, J. S. Gutmann and K. Mullen, *Angew. Chem., Int. Ed.*, 2008, **47**, 8400–8403.
6 C. J. Jia, L. D. Sun, F. Luo, X. D. Han, L. J. Heyderman, Z. G. Yan, C. H. Yan, K. Zheng, Z. Zhang, M. Takano, N. Hayashi, M. Eltschka, M. Klaui, U. Rudiger, T. Kasama, L. Cervera-Gontard, R. E. Dunin-Borkowski, G. Tzvetkov and J. Raabe, *J. Am. Chem. Soc.*, 2008, **130**, 16968–16977.
7 X. Peng, J. Chen, J. A. Misewich and S. S. Wong, *Chem. Soc. Rev.*, 2009, **38**, 1076–1098.
8 M. Wang, X. Zhang, Q. S. Zheng and Y. Liu, *Nanotechnology*, 2007, **18**, 375706.
9 X. B. Yan, Z. J. Han, Y. Yang and B. K. Tay, *J. Phys. Chem. C*, 2007, **111**, 4125–4131.
10 E. Castillejos, P. J. Debouttiere, L. Roiban, A. Solhy, V. Martinez, Y. Kihn, O. Ersen, K. Philippot, B. Chaudret and P. Serp, *Angew. Chem., Int. Ed.*, 2009, **48**, 2529–2533.
11 T. Koishi, S. Yoo, K. Yasuoka, X. C. Zeng, T. Narumi, R. Susukita, A. Kawai, H. Furusawa, A. Suenaga, N. Okimoto, N. Futatsugi and T. Ebisuzaki, *Phys. Rev. Lett.*, 2004, **93**, 185701.
12 Z. X. Cai and X. P. Yan, *Nanotechnology*, 2006, **17**, 4212–4216.
13 G. H. Lu, L. Y. Zhu, P. X. Wang, J. H. Chen, D. A. Dikin, R. S. Ruoff, Y. Yu and Z. F. Ren, *J. Phys. Chem. C*, 2007, **111**, 17919–17922.
14 M. M. Rabbani, C. H. Ko, J. S. Bae, J. H. Yeum, I. S. Kim and W. Oh, *Colloids Surf., A*, 2009, **336**, 183–186.
15 B. Kim, H. Park and W. M. Sigmund, *Langmuir*, 2003, **19**, 2525–2527.
16 K. Y. Jiang, A. Eitan, L. S. Schadler, P. M. Ajayan, R. W. Siegel, N. Grobert, M. Mayne, M. Reyes-Reyes, H. Terrones and M. Terrones, *Nano Lett.*, 2003, **3**, 275–277.
17 M. A. Correa-Duarte and L. M. Liz-Marzan, *J. Mater. Chem.*, 2006, **16**, 22–25.
18 B. F. Pan, D. X. Cui, C. S. Ozkan, M. Ozkan, P. Xu, T. Huang, F. T. Liu, H. Chen, Q. Li, R. He and F. Gao, *J. Phys. Chem. C*, 2008, **112**, 939–944.
19 S. H. Baek, B. Kim and K. D. Suh, *Colloids Surf., A*, 2008, **316**, 292–296.
20 L. Wang, S. J. Guo, X. O. Hu and S. J. Dong, *Colloids Surf., A*, 2008, **317**, 394–399.
21 S. Jaffar, K. T. Nam, A. Khademhosseini, J. Xing, R. S. Langer and A. M. Belcher, *Nano Lett.*, 2004, **4**, 1421–1425.
22 V. Panchagnula, J. Jeon and A. V. Dobrynin, *Phys. Rev. Lett.*, 2004, **93**, 037801.
23 A. B. Artyukhin, O. Bakajin, P. Stroeve and A. Noy, *Langmuir*, 2004, **20**, 1442–1448.
24 D. V. Bavykin, A. A. Lapkin, P. K. Plucinski, L. Torrente-Murciano, J. M. Friedrich and F. C. Walsh, *Top. Catal.*, 2006, **39**, 151–160.
25 F. C. Walsh, D. V. Bavykin, L. Torrente-Murciano, A. A. Lapkin and B. A. Cressey, *Trans. Inst. Met. Finish.*, 2006, **84**, 293–299.
26 X. Chen and S. S. Mao, *Chem. Rev.*, 2007, **107**, 2891–2959.
27 Q. Chen, G. H. Du, S. Zhang and L. M. Peng, *Acta Crystallogr., Sect. B: Struct. Sci.*, 2002, **58**, 587–593.
28 X. M. Sun and Y. D. Li, *Chem.–Eur. J.*, 2003, **9**, 2229–2238.
29 H. Y. Zhu, Y. Lan, X. P. Gao, S. P. Ringer, Z. F. Zheng, D. Y. Song and J. C. Zhao, *J. Am. Chem. Soc.*, 2005, **127**, 6730–6736.
30 Y. Lan, X. P. Gao, H. Y. Zhu, Z. F. Zheng, T. Y. Yan, F. Wu, S. P. Ringer and D. Y. Song, *Adv. Funct. Mater.*, 2005, **15**, 1310–1318.
31 T. Kasuga, M. Hiramatsu, A. Hoson, T. Sekino and K. Niihara, *Langmuir*, 1998, **14**, 3160–3163.
32 T. Kasuga, M. Hiramatsu, A. Hoson, T. Sekino and K. Niihara, *Adv. Mater.*, 1999, **11**, 1307.
33 K. Shankar, J. I. Basham, N. K. Allam, O. K. Varghese, G. K. Mor, X. J. Feng, M. Paulose, J. A. Seabold, K. S. Choi and C. A. Grimes, *J. Phys. Chem. C*, 2009, **113**, 6327–6359.
34 H. B. Li, X. C. Duan, G. C. Liu and X. Q. Liu, *J. Mater. Sci.*, 2008, **43**, 1669–1676.
35 B. L. Zhu, Z. M. Sui, S. R. Wang, X. Chen, S. M. Zhang, S. H. Wu and W. P. Huang, *Mater. Res. Bull.*, 2006, **41**, 1097–1104.
36 P. P. Das, S. K. Mohapatra and M. Misra, *J. Phys. D: Appl. Phys.*, 2008, **41**, 245103.
37 I. Paramasivalm, J. M. Macak and P. Schmuki, *Electrochem. Commun.*, 2008, **10**, 71–75.
38 J. W. Slot and H. J. Geuze, *Eur. J. Cell Biol.*, 1985, **38**, 87–93.
39 V. J. Gandubert and R. B. Lennox, *Langmuir*, 2005, **21**, 6532–6539.
40 D. V. Bavykin, V. N. Parmon, A. A. Lapkin and F. C. Walsh, *J. Mater. Chem.*, 2004, **14**, 3370–3377.
41 S. Kumar, K. S. Gandhi and R. Kumar, *Ind. Eng. Chem. Res.*, 2007, **46**, 3128–3136.

 This journal is © The Royal Society of Chemistry 2009

View Article Online

42 T. Zhu, K. Vasilev, M. Kreiter, S. Mittler and W. Knoll, *Langmuir*, 2003, **19**, 9518–9525.
43 J. Turkevich, P. C. Stevenson and J. Hillier, *Discuss. Faraday Soc.*, 1951.
44 G. Frens, *Nat. Phys. Sci.*, 1973, **241**, 20–22.
45 D. I. Gittins and F. Caruso, *Angew. Chem., Int. Ed.*, 2001, **40**, 3001–3004.
46 D. V. Bavykin, J. M. Friedrich, A. A. Lapkin and F. C. Walsh, *Chem. Mater.*, 2006, **18**, 1124–1129.
47 S. K. Ghosh and T. Pal, *Chem. Rev.*, 2007, **107**, 4797–4862.
48 C. A. Mirkin, R. L. Letsinger, R. C. Mucic and J. J. Storhoff, *Nature*, 1996, **382**, 607–609.
49 S. Y. Park, A. K. R. Lytton-Jean, B. Lee, S. Weigand, G. C. Schatz and C. A. Mirkin, *Nature*, 2008, **451**, 553–556.
50 J. J. Storhoff, A. A. Lazarides, R. C. Mucic, C. A. Mirkin, R. L. Letsinger and G. C. Schatz, *J. Am. Chem. Soc.*, 2000, **122**, 4640–4650.
51 J. Schmitt, G. Decher, W. J. Dressick, S. L. Brandow, R. E. Geer, R. Shashidhar and J. M. Calvert, *Adv. Mater.*, 1997, **9**, 61.
52 C. P. Collier, R. J. Saykally, J. J. Shiang, S. E. Henrichs and J. R. Heath, *Science*, 1997, **277**, 1978–1981.

Published on 19 October 2009. Downloaded by Michigan State University on 29/01/2016 16:37:24.